Photogrammetric Deflection Measurements for the Tiltrotor Test Rig (TTR) Multi-Component Rotor Balance Calibration

Eduardo Solis
Research Engineer
Monterey Technologies, Inc
Moffett Field, CA, U.S

Larry Meyn
Mechanical Engineer
NASA Ames Research Center
Moffett Field, CA U.S

ABSTRACT

Calibrating the internal, multi-component balance mounted in the Tiltrotor Test Rig (TTR) required photogrammetric measurements to determine the location and orientation of forces applied to the balance. The TTR, with the balance and calibration hardware attached, was mounted in a custom calibration stand. Calibration loads were applied using eleven hydraulic actuators, operating in tension only, that were attached to the forward frame of the calibration stand and the TTR calibration hardware via linkages with in-line load cells. Before the linkages were installed, photogrammetry was used to determine the location of the linkage attachment points on the forward frame and on the TTR calibration hardware. Photogrammetric measurements were used to determine the displacement of the linkage attachment points on the TTR due to deflection of the hardware under applied loads. These measurements represent the first photogrammetric deflection measurements to be made to support 6-component rotor balance calibration. This paper describes the design of the TTR and the calibration hardware, and presents the development, set-up and use of the photogrammetry system, along with some selected measurement results.

NOTATION

AFP	=	positive axial force, along the x-axis
AFN	=	negative axial force, along the x-axis
NFP	=	positive normal force, along the z-axis
PMP	=	positive pitch moment, about the y-axis
PMN	=	negative pitch moment, about the y-axis
RMP	=	positive roll moment, about the x-axis
RMN	=	negative roll moment, about the x-axis
SFP	=	positive side force, along the y-axis
SFN	=	negative side force, along the y-axis
TQS	=	positive torque starboard, about the z-axis
TQP	=	positive torque port, about the z-axis

ABBREVIATIONS

TTR	Tiltrotor Test Rig
RTA	Rotor Test Apparatus
LRTA	Large Rotor Test Apparatus
NFAC	National Full-Scale Aerodynamics Complex
V-STARS	Video-Simultaneous Triangulation and Resection System
V-STARS/S	single camera system
V-STARS/M	dual-camera system
ROI	region of interest
DOF	degrees of freedom
DOE	design of experiment

Presented at the 2016 AHS Technical Meeting on Aeromechanics Design for Vertical Lift, San Francisco, California, January 20-22, 2016.

INTRODUCTION

The Tiltrotor Test Rig (TTR) is a national facility that will enable advanced, large-scale tiltrotor technology testing at speeds up to 300 kts. The TTR, a NASA project joint with the Army and Air Force, can test proprotors up to 26 ft in diameter in the National Full-Scale Aerodynamic Complex (NFAC).

The TTR is designed for use in the NFAC's 40- by 80- and the 80- by 120-Foot wind tunnels. The TTR is a horizontal axis rig that mounts on the test-section turntable, enabling testing at high speeds (300 knots) in axial flight or edgewise flight at low speeds (180 knots), or at any angle in between as shown in Fig. 1. The TTR is designed to accommodate a variety of rotor types: articulated, gimbaled, soft-in plane, and rigid rotors up to 26-feet in diameter. The power, speed and aerodynamic load capabilities of the TTR are necessary to provide critical data to validate state-of-the-art design and analytical tools needed to develop future advanced rotorcraft concepts. To keep pace with the progress in higher fidelity computational tools, methods for improving the accuracy of rotor performance measurements are required.

The first test entry for the TTR is a system validation test using an existing research rotor in the 40- by 80- test section. The TTR must go through a series of system and hardware checkouts before this initial test entry (planned for 2016). Most importantly, the internal multi-component rotor balance must be calibrated to accurately measure the total forces and moments generated by the rotor system.

Large-scale multi-component rotor balance calibrations have long been a challenge to the rotorcraft community. The challenge of both measuring hardware deflections and

minimizing hardware misalignment to reduce balance calibration uncertainty is not new, but a standard approach has not been fully developed for large-scale test rigs. NASA developed the Rotor Test Apparatus (RTA) in the mid 1970's and the Large Rotor Test Apparatus (LRTA) in the 1990's to test small-and large-scale rotor systems as described in Refs. 1-3. Based upon the RTA experience, rotor balance bench calibrations may not adequately represent installed balance behavior, and so calibrations should be performed in-place (Ref. 1). The LRTA included the design of a calibration stand, which enabled an LRTA in-place rotor balance calibration. Deflection measurements using a laser tracker were acquired during the LRTA balance calibration. The applied calibration loadings were corrected with the deflection measurements as described in Ref. 2. The orientation and the complex design of the LRTA calibration stand and calibration hardware limited the deflection measurements to one rotor quadrant of the loading tree.

A multi-component balance calibration was performed on the TTR to enhance NASA's capability to accurately measure rotor performance for full-scale rotor tests. To improve on the previous balance calibration methods as discussed in Refs. 1-3, the TTR balance calibration utilized photogrammetry techniques to measure/reduce load misalignment and to measure system deflections under load. First, photogrammetric measurements were used to guide and evaluate efforts to reduce the loading hardware misalignment. The goal was to reduce misalignments to under +/-0.06 inches, in order to minimize off-axis components from applied loads. The second use was to measure the system deflections under load, during the calibration. By measuring the deflected location of all applied loads to within +/-0.05 inches, the uncertainty in the magnitudes of the estimated off-axis forces from the applied loads could be kept to less than 5 lbs.

This paper describes the calibration rig, TTR rotor balance, and the photogrammetric measurement system. The overall calibration system design was largely driven by the constraints imposed by the TTR and the calibration hardware. These constraints and other challenges are discussed, along with some selected measurement results.

CALIBRATION SYSTEM DESCRIPTION

To simulate the range of rotor forces and moments on the TTR, NASA designed calibration hardware to apply loads to the rotor shaft and the internal rotor balance as shown in Fig. 2.

To accurately calibrate the rotor balance, the actuators must be aligned with the metric hardware to minimize force interactions as shown in Fig. 3. Deflection measurements of the rotor shaft and metric hardware under load are necessary to accurately determine the location and direction of applied loads, since an inch of deflection could result in off-axis forces in excess of 100 lb.

The major components of the calibration system are: the calibration stand, the calibration body, the hydraulic actuator load system (attached to the FWD Frame), the data acquisition system, and the photogrammetry system.

The calibration stand consists of two subassemblies, the FWD Frame and the AFT Frame. The FWD Frame provides a rigid support for the non-metric end of the hydraulic actuators. The AFT Frame provides rigid support for the TTR. The TTR is attached to the AFT Frame on three struts using a ball-socket interface. The FWD Frame and the AFT Frame are bolted to each other at the base and at the interface beam attachment points. The interface beams provide structural support to minimize deflection when applying single-and multi-component loads to the TTR. Figure 2 shows the TTR installed on the calibration stand.

The calibration body consists of the TTR, the rotor balance, and the metric hardware as shown in Fig. 3. The metric hardware is designed to apply known forces and moments to the rotor balance and rotor shaft.

The loading system consists of the anchor hardware, the metric hardware, and the interface hardware, which provides the mechanical connection between the calibration frame and the calibration body. Assembly of the interface hardware includes a load cell, tension tube, actuator and a clevis as shown in figure 3. The anchor hardware is mounted on the FWD Frame and provides the structural housing for the actuator. A total of eleven linkages with in-line load cells and hydraulic actuators, operating in tension only, were used to apply the calibration loads as shown in Fig. 3 and Fig. 13 (close-up view).

The metric hardware provides the interface between the load actuators and the rotor shaft, and allows for two calibration ranges: the expected load range for the first wind tunnel test entry and the design load range of the rotor balance. In order to apply the two calibration ranges, the metric hardware was designed to allow for three base hardware configurations. For configuration 1, normal force and torque loads are applied to the rotor shaft and all other loads are applied to the balance. In configuration 2, no loads are applied to the rotor shaft while loads are applied to the balance. In configuration 3, normal force, torque and shear loads are applied to the rotor shaft and all other loads are applied to the balance. Side views of the three hardware configurations is shown in Fig. 4.

ROTOR BALANCE DESCRIPTION

The TTR has an in-place six-component, non-rotating, rotor balance as shown in Fig. 5 and Fig. 6 (close-up view). However, since rotor torque is provided by a rotating drive train, torque is measured by instrumentation on a torque tube, which is installed as part of the drive train. The balance and the torque tube are both shown in Fig. 7, which depicts the TTR drive train from the gearbox to the client mast. A necked down portion of the torque tube is instrumented with two gages to provide primary and secondary (backup)

measurements of torque. The torque tube and instrumentation is rated to 22,338 ft-lb. Thrust from the rotor is primarily measured by the non-rotating balance. However, this balance measurement must be corrected for small residual forces from the drive train, due to thermal expansion and reactions to applied torque. Instrumentation on the torque tube diaphragm provides primary and secondary measurements of the components of these residual forces that are aligned with thrust. The rotor balance has a capacity of 30,000 lb in thrust, 16,000 lb in shear force and 149,333 ft-lb in combined roll and pitch moments about the balance center. These balance capacity limits include forces and moments due to hardware weight. Table 1 shows the calibration range for the TTR rotor balance. These values are for forces and moments applied at the center of the rotor hub, which is 88 in. forward of the balance center, and do not include any contributions due to hardware weight (up to 6000 lb). It should be noted that shear forces applied at the hub result in moments about the balance center. Figure 5 shows the TTR calibration-reference axis system.

Table 1. Rotor Balance Calibration Ranges

Load (applied at the hub)	Research Rotor Calibration Range	Balance Design Range
Normal Force	**15,184 lb**	**30,000 lb**
In-plane Shear	**8250 lb**	**10,000 lb**
Hub Moment	**7500 ft-lb**	**60,000 ft-lb**
Torque	**22,338 ft-lb**	**22,338 ft-lb**

PHOTOGRAMMETRY SYSTEM DESCRIPTION

Photogrammetry is the science of making 3D location measurements from photographs and images. The photogrammetry system used was based on Geodetic Systems, Inc.'s portable Video-Simultaneous Triangulation and Resection System (V-STARS®)[1] software and hardware. These system components were selected for their ability to obtain highly accurate measurements of large, complicated objects, such as the TTR, the calibration stand and calibration hardware.

The V-STARS system consists of a workstation computer and two ultra-high-resolution digital cameras. The system measures the 3-dimensional coordinates of points of interest by intersecting the lines of sight from the cameras to the points using a process called triangulation, which follows the single camera photogrammetry principle as discussed in Refs. 4 - 6.

[1]Geodetic Systems, Inc, http://geodetic.com, Melbourne, FL
[2]Trimble Navigation, http://sketchup.com, Sunnyvale, CA

The V-STARS software supports two camera systems: the V-STARS/S system and the V-STARS/M system. The V-STARS/S is a single camera system and was used to align the calibration hardware and develop the control field (calibration files) for the V-STARS/M system. The 3D measurement accuracy of current V-STARS/S systems ranges from 10 µm + 10 µm/m to a maximum of 5 µm + 5 µm/m, the latter accuracy corresponding to 0.001" @ 160" or 1:160,000.

The V-STARS/M is a dual-camera system and was used to acquire real-time deflection measurements during balance calibration. One of the most powerful features of the dual-camera system is its ability to measure in unstable environments by setting the system to Unstable Mode. The Unstable Mode makes use of stable, targeted control points that were placed on the FWD Frame. The V-STARS/M system uses these stable, targeted control points to calculate the position and orientation of the cameras each time a deflection measurement is made. Thus, movement of the cameras and the test rig is accounted for in every picture and has no effect on system accuracy. The coordinates for these points were established by a one-time single-camera measurement to create the control field for the dual-camera system. The unstable mode combined with the synchronized strobes enables the system to make accurate measurements if vibrations are present during calibration loads. The dual camera, real-time V-STARS/M measurement system produces an accuracy of 14 µm + 14 µm/m or 1:60,000 on a 4m object (0.003" @ 160").

PHOTOGRAMMETRY METHODOLOGY

The photogrammetry system development was initiated and completed prior to buildup of the calibration stand and installation of the TTR. Development utilized 3D modeling software for the determination of camera and target positions. In addition, all potential camera positions were screened to ensure that they met the 60-degree apex-angle required for the V-STARS/M system as discussed in Ref. 7.

Approach

3D Computer Aided Design (CAD) models of the TTR, the calibration stand and the calibration hardware were created and imported into SketchUp[2], a 3D modeling program. In addition, a camera lens model was created and imported into SketchUp to model the V-STARS cameras' fields of view. The 3D model was used to determine nominal camera locations and the camera lens model identified the visual blockage imposed by the TTR, the calibration stand and calibration hardware. The lens model also identified the placement of targets on the metric hardware where both cameras have a line of sight to all the targets, which is required for the dual-camera system to acquire deflection measurements.

For verification of the nominal camera positions identified in the 3D model, a full system checkout of the V-STARS/M system was completed, which included a full-scale foam

model of the metric hardware. The TTR, the calibration stand, the calibration hardware, and camera support stand were not yet available to complete a system checkout. Therefore, a foam model of the metric hardware was built to mirror the setup from the 3D SketchUp model to place and access the cameras on the ground floor. The foam model was used to design the photogrammetry alignment and deflection hardware, determine retro-reflective target size, and verify the camera stations and apex-angle. Figure 8 shows the full-scale foam model and the V-STARS/M system in the lab. A final checkout was completed using the camera support structure after the TTR was installed on the calibration stand.

Photogrammetry Setup

To prepare the calibration hardware for photogrammetric measurements, special retro-reflective targets were installed on the FWD Frame and the calibration body. Retro-reflective targets provide the necessary contrast needed to accurately identify targets in photogrammetry images. The target material was 4-mil thick, 3M Scotchlite 7610, high-reflectance adhesive tape. To acquire accurate measurements during the calibration process, a minimum of 20 targets (points) and 4 coded targets were required in each measurement image acquired. To satisfy the V-STARS minimum requirements and overcome the visual constraints imposed by the calibration hardware buildup, a total of 2,800 3/8-inch diameter retro-reflective targets and 120 coded targets were evenly (approximately) installed all around the inner faces of the FWD Frame, the calibration body, the TTR, and the rotor balance.

An Autobar and two carbon-fiber scale bars (3-m long), were used to define the preliminary origin and set the volumetric scale. The rotor balance coordinate system served as the global origin for all photogrammetric measurements. The coordinate system was established using four equally and radially spaced pin holes located on the base of the rotor balance as shown in Fig. 6. The flange was the closest accessible feature to the balance origin with known dimensions. Four custom-machined, retro-reflective steel button targets were pressed into the pin holes. The custom targets were machined with an accuracy of +/- 0.0005 in to reduce hardware buildup error. The four targets were used to transpose the origin of all alignment measurements to the balance coordinate system.

Alignment Hardware Setup

The interface hardware attachment points located on the FWD Frame were aligned to the metric hardware attachments points so that the loads applied to the calibration body would be nearly parallel to the principal axes of the balance coordinate system. The interface hardware was removed during alignment measurements so that the attachment points were visible and to allow adjustment of the anchor hardware, which is the structural housing for the actuator attachment hardware.

The complex buildup of the calibration stand, the calibration hardware, the TTR, and the instrumentation cables imposed severe visual constraints. Therefore, special alignment hardware was designed and built to place visible alignment targets in precise, offset positions to locate the linkage attachment points. The load application points on the calibration body and the linkage attachment points on the calibration frame were measured and documented using the photogrammetry technique to determine the load vector for each actuator fixed in space.

The alignment hardware consisted of several components: the horizontal cross bar, the target holder, custom button targets, adhesive retro-reflective targets and two alignment plates. The target holder screws into the plug of each anchor and places a retro-reflective target centroid at the linkage attachment point, perpendicular to the load vector as shown in Fig. 9.

On the metric hardware, a single target could not be installed into the pitch and roll moment linkage attachment points, therefore two targets were used to interpolate the center of the linkage. The interpolation was accomplished by installing custom buttons with vertically-flush targets into the linkage attachment on each side of the moment arm as shown in Fig. 10. Heavy-duty magnets were used in between the button targets to prevent the hardware from falling out. To align axial and side force attachment points, button targets were installed onto the shear blocks as shown in Fig. 10. For the normal force attachment point, a target holder was installed on the thrust adaptor plate attachment point as show in Fig. 11.

Torque loads were applied using chains on a sprocket gear. The chain and sprocket system ensured that loads were applied at points tangent to the sprocket. These tangent points were determined by the center of the sprocket, the diameter of the sprocket and the orientation of the sprocket's plane of rotation. The values were determined using measurements of adhesive 3/8-in diameter retro-reflective targets that were installed on every other tooth and on both sides of the torque sprocket.

Two alignment plates measuring 12 x 12 x 0.25 inches and 6 x 12 x 0.25 inches were installed on the calibration body. Except for the size difference, the alignment plates were similar in design. Each plate is made from MIC 6 aluminum tooling plate and have flush and counter-sunk ¼-inch diameter retro-reflective targets. The 12x12 inch alignment plate was installed on the thrust adaptor plate and the 6x12 inch alignment plate was installed on the axial negative force block as shown in Fig. 11. The alignment plates were leveled with an inclinometer before the start of each photogrammetry shoot. The alignment plates provided multiple targets on a flat plane that were used to move the origin within the software for alignment verification when combining multiple shoots into one.

Misalignment Measurement Process

Over a two-week period, three iterations of hardware adjustment and photogrammetric measurements were completed to reduce the misalignment between the anchor hardware and metric hardware attachment points. The initial goal to align the linkage attachment points was +/-0.06 inches, but due to the constraints imposed by the anchor hardware and FWD Frame and limited time, not all anchors were aligned within the threshold. Most importantly, the XYZ location of the linkage attachment points was measured relative to the balance origin including misalignments. Figure 12 shows the final triangulation of the measured points.

Deflection Hardware Setup

The photogrammetric setup to measure the control field for the deflections measurements was more difficult than the setup for misalignment measurements, as the interface hardware was installed and the linkage attachment points on the metric hardware were blocked from view. To deal with this issue, deflection hardware was designed so that retro-reflective targets could be installed to interpolate the linkage attachment points on the calibration body. This was not feasible for attachment points on the FWD Frame, so they could not be measured during calibration. However, the FWD Frame was designed so that deflections under calibration loads would be insignificant.

The deflection hardware consists of precision-machined components: the extension brackets, the deflection cross, and frames constructed of modular aluminum T-slot framing from 80/20® Inc[3]. The design was driven by the hardware buildup between the interface hardware and metric hardware shown in Fig. 13. The majority of the hardware was designed during the bench calibration of the V-STARS/M system.

A total of eight extension brackets were installed on the metric hardware: two for each moment arm. The extension brackets were a two-piece design comprised of a support frame and an extension. The support frame was bolted to the moment arm with tight-fitting hardware to remove slop. The extension was located at the center of the support frame with a swivel bolt, and can support up to five flush targets. The extension brackets were designed to place 3/8-inch diameter retro-reflective targets at equal distance on each side of the moment arm as shown in Fig. 14. The software can then compute an interpolated point at the linkage attachment point. The extension allows for the retro-reflective targets to rotate in-line with the axis between the two targets as shown in Fig. 15. The target viewing angle for each camera is therefore improved, increasing target reflectivity, which improves centroid accuracy. These extension brackets were used to interpolate the linkage attachment points for pitch moment and roll moment. In addition, the targets were combined together to interpolate the center of the metric hardware.

[3] 80/20 Inc., https://8020.net, Columbia City, IN

The deflection cross was installed on the thrust adaptor plate for measuring deflections due to torque and shear loads on the rotor shaft and torque on the metric hardware. Custom button targets were installed at the end of each cross arm. The deflection cross was designed to allow for radial and forward adjustment of the button targets to avoid blocking the camera view. In addition, the carbon fiber tubes holding the button targets allowed the targets to rotate in order to improve the viewing angle of the targets for each camera. Figure 16 shows the design of the deflection cross.

Half-inch diameter adhesive retro-reflective targets were installed on the aft face of the moment arms. These targets were used to determine the orientation of the metric hardware, and create the control field for the dual-camera system.

The 80/20 hardware was installed on the upper two rotor quadrants and at the base of the FWD Frame as shown in Fig. 17. The 80/20 hardware was bolted and clamped to the I-beams in tension to prevent movement when vibrations were present. Thirty 5-in square steel plates were installed on the 80/20 hardware with one bolt and a locking washer. Coded targets were installed on the steel plates using heavy-duty adhesive magnets. In addition to the coded targets, three ½-in diameter adhesive retro-reflective targets were installed on each plate in order to have 256 reference points for the V-STARS/M system (the system requires a minimum of 50 reference points). The X and Y position of the coded targets were manually adjustable to ensure the coded targets were visible by both cameras during deflection measurements. In addition, the 80/20 support frame was installed at an angle to place the coded targets out-of-plane to increase the calibration volume in the Z-direction. Figure 17 shows the installation of the deflection targets.

Dual-Camera System Setup

Two identical cameras were used to acquire deflection measurements during balance calibration. Each camera has a 2K x 2K sensor, a 21-mm lens (fixed focal length) and a flash ring. The cameras were synchronized with the following settings: flash power = 9, shutter speed = 0.1 s, and f-stop = 18.

Two support structures, one for each camera were installed on each side of the TTR. The support structure for each camera included an off-the-shelf 16-ft high aluminum staging truss, a camera boom, a tilt-head, and three steel cables. The support structure placed the cameras nominally 19-ft above the ground. The aluminum staging trusses were selected for their light weight construction, solid conical connectors and tapered pins for quick and secure assembly. The trusses were bolted to the steel floor and three steel cables were tethered from the top of the truss to the floor for added rigidity at the camera locations. The camera boom allowed for coarse camera adjustment and the tilt-head mounted at the end of the boom provided a finer camera adjustment. The combination of the camera boom and the tilt-head provided six degrees of freedom (DOF) of movement. The 6 DOF allowed the

cameras to be adjusted to avoid blockage (electronic hardware and cables) that was not modeled in the 3D SketchUp model. The camera support structure is shown in Fig. 18.

The camera support structures were installed 12-ft apart from each other and 12-ft aft of the metric hardware. The spacing between the support structures in combination with the camera boom ensured the optical axes of the cameras intersected at an angle between 60 and 65 degrees, which is the optimum apex-angle for the V-STARS/M system as described in Ref. 7. Figure 19 shows a plan view of the camera locations.

The cables to power and remotely trigger the cameras were routed from the top of the trusses to the control box located on the first floor next to the TTR. The control box provided clean power to the cameras and filtered out electronic noise. An RJ-45 cable was routed from the control box to the control room. The cameras were remotely triggered from the control room with a workstation laptop.

Deflection Measurement Process

During balance calibration, each load condition was applied for 30 seconds. The deflection measurement was manually triggered 10 seconds into each load condition and two image pairs and a triangulation file were acquired for each applied load point. The measured points were quickly scanned before proceeding to the next load condition. The photogrammetry system acquired 4,002 load measurements during the rotor balance calibration period, which included three base hardware configurations and six extended load configurations for diagnostic checks.

CAMERA CALIBRATION

Single Camera

The single camera system required multiple steps to maintain the camera self-calibration in order to acquire accurate measurements of the retro-reflective targets.

The first step involves focusing and setting the correct exposure to easily find and measure the targets. The second step requires the camera to be rolled (90-deg) for half of the measurements in order for the camera to self-calibrate. Lastly, the V-STARS software requires coded targets, an Autobar, and two scale bars in order to triangulate the position of the targets and set the scale for the 3D measurements.

The single camera system has a 24-mm wide angle (fixed focal length) lens and was designed to focus on points between 0.5 m (20 in) and 60 m (200 ft) from the camera, effectively eliminating the depth of focus problem. The depth of field permitted placement of retro-reflective targets all around the FWD Frame and calibration body.

Retro-reflective targets were selected to insure that the target and the background exposures were independent of each other. The target exposure is determined by the power of the ring flash, while the background exposure is determined by the ambient lighting, which is controlled by the shutter speed. The goal is to have bright, but not saturated, target images that are easily distinguished from the background. Several test shots with different strobe power and shutter settings were tested to improve the exposure of the retro-reflective targets against the gloss white paint of the FWD Frame, the TTR body and the bare metal hardware. For each test shot, the grayscale values for each target were inspected to verify the target was not over- or under-exposed.

To self-calibrate the camera during misalignment measurements, the camera was rolled 90-deg for every other picture taken. Rolling the camera calibrated the camera at the time of measurement, which is far superior to relying on lab calibrations. In addition, multiple camera stations were screened prior to the start of the misalignment measurements. Eight to ten pictures were acquired for each camera station.

For improved accuracy, the coded targets, an Autobar, and two scale bars were used during photogrammetry measurements. The coded targets are used to stitch the images together when the data is processed, the Autobar defines the global coordinate system, and the scale bars are used to set the scale for all 3D measurements. The software then determines the final orientation of the camera stations in order to triangulate the measured targets.

To verify the accuracy of the camera settings and photogrammetric setup, the scale bars and the Autobar measured values were compared to the calibration certificates.

Dual-Camera

For the dual-camera system, the camera calibration required a four-step process to develop the control field.

The first step involved setting up the V-STARS hardware on the calibration body, which includes: coded targets, an Auto bar, and two scale-bars to meet the V-STARS system requirements.

During the second step, all the points on the calibration body and 80/20 hardware were measured. Images were captured all around the calibration body and processed. To verify the measurements were accurate and to scale, the scale bars and the Autobar measured values were compared to the calibration certificates.

The third step involved culling the data and verifying all the critical points were captured with an acceptable accuracy. The unwanted scans (orphan points) were globally deleted and the image set was reprocessed. After the aforementioned was completed, the coded targets, the Auto bar, and two scale bars

were carefully removed from the calibration body. In addition, the fill-in targets were covered.

Lastly, to create the control field for the dual camera system. The Autobar origin was transposed to the balance origin using the four points located at the base of the rotor balance. After the global origin was transposed, the points for the coded targets, the Auto bar, and the two scale bars were removed. The control field was then separated into two sets of points; the detail points and driver points. The detail file only included the points that were installed on the metric hardware. The driver file included all the points on the 80/20® hardware that were used as the reference points for camera orientation. To verify the accuracy of the control field, 50 static images were taken before and after each calibration run. The accuracy for each measured point was used to verify the accuracy of the control field before, during, and after each calibration run. Figure 20 shows the driver and detail points.

The control field was measured once a week and after each hardware configuration change. In addition, the V-STARS/M system was set to unstable mode and the strobe power and shutter speed for each camera were synchronized to maintain system accuracy throughout the entire calibration process.

CHALLENGES

Acquiring photogrammetric measurements was difficult due to the construction and buildup of the calibration stand and calibration hardware. A 21-mm viewfinder was used to study the blockage and determine the camera stations for the misalignment measurements and to generate the control field. The camera stations were marked on the ground and the vertical positions were dictated by the surrounding hardware.

To verify each camera station, the wireless card on the camera was used to communicate with the computer. The wireless card provided real-time measurements and allowed for quick validation. To validate each camera station, a minimum of 6 coded targets and 20 individual targets were required for each picture taken.

The camera viewfinder was not used for all camera stations. Instead, laser pointers were used in small, tight areas to align the optical axis of the camera to a cluster of targets. Marking the camera stations and using the wireless card with the laser pointers yielded repeatable measurements and consistent accuracy throughout the entire calibration phase. Figure 21 shows the camera stations used for the misalignment measurements and for generating the control field.

In the early stages of the deflection measurements, during configuration 1, the region of interest (ROI) of two targets would appear very close to each other under large deflections. As a result, the software would incorrectly swap the labels of the two targets. To mitigate the problem, a dedicated loading sequence with large deflections was developed to test possible solutions. As a result, the inner targets for each arm were removed to avoid target mislabeling and the ROI of the outer-most target was increased in order to capture the target at its largest displacement (when applying 5,930 ft-lb of torque to the rotor shaft).

In configuration 2, several points yielded high alignment errors. Upon further investigation, the system was found to register metal shavings and glossy paint highlights as targets that were in close proximity to the retro-reflective targets. These false targets caused the centroid of each true target to shift, resulting in high errors. To mitigate the problem, a black pen was used to cover the highlights on multiple locations of the metric hardware and the FWD Frame. In addition, the floors were vacuumed to remove debris.

DATA PROCESSING

The location and direction of forces applied to the balance was based on the estimated positions of the linkage attachment points shown in Fig. 12. These positions were measured statically before and after the calibration without the linkages installed, as described previously. Given the strength and rigidity of the FWD Frame structure, the attachment points on the FWD Frame were assumed to be stationary when calibration loads were applied.

During the calibration, the locations of the linkage attachment points on the TTR metric hardware were estimated using photogrammetric measurements of the targets shown in Fig. 22. The V-STARS software determined the moment arm attachment points by averaging the locations of the targets on the extension brackets mounted on both sides of each attachment point. However, the locations of the other attachment points were determined during further post-processing using data exported from the V-STARS software.

The remaining linkage attachment point locations were estimated using the four targets on the cross mounted to the sprocket hardware (Fig. 16). For each calibration load, these four target locations, along with their zero load locations, were used to determine 3D rotation and translation parameters that describe the change in position and orientation of the sprocket hardware under load. The full set of rotation and translation parameters were applied to reference locations of the axial and side force attachment points on the TTR metric hardware. Since the torque attachment points were tangential to the sprocket, even when the sprocket rotated about the z-axis, the parameter for rotation about the z-axis was set to zero before applying the sprocket rotations and translations to the torque attachment point locations. Lastly, the normal force attachment point was assumed to have the same translations and not rigidly rotate with the sprocket hardware, so only the sprocket translation parameters were applied to the normal force attachment point location.

The possibility exists that the position and orientation of the balance center may also change under load. A method was developed to estimate these changes using additional photogrammetry data that was obtained during the calibration, but a description of that process is beyond the scope of this paper.

RESULTS

Misalignment Measurements

The misalignment of the actuators should be reduced to enable pure loads, but due to size, weight, and physical access to the anchor hardware, misalignment of the actuators within +/- 0.06 in proved difficult. Most important, the 3D positions of the linkage attachment points were measured in the balance coordinate system. This enabled deflection measurements of the calibration body used to determine the location and direction of forces applied to the rotor balance.

Table 3 shows the pre-balance calibration misalignment measurement results before the start of the balance calibration. Table 4 shows the post-balance calibration misalignment measurement results three months later. Table 5 shows the average results between the pre-balance and post-balance calibration misalignment measurements. The estimated misalignment results in table 5 were used to adjust the data to account for misalignment.

Deflection Measurements

Deflection measurements of all targets were successfully acquired for all three hardware configurations. Figure 23 shows the deflection sequence for the pitch moment (positive) interpolated point for all load combinations in configuration 1. The data shows more movement than expected, up to half an inch lateral movement, which is too much to ignore in the calibration process. The maximum deflection for each linkage attachment point over all configurations is presented in Table 2.

Table 2. Maximum Attachment Point Deflections

Actuator	ΔX (in)	ΔY (in)	ΔZ (in)
NFP	1.10	1.04	0.32
SFN	1.42	0.80	0.31
SFP	1.33	0.79	0.24
AFN	0.86	1.37	0.26
AFP	0.86	1.29	0.26
RMN	0.39	0.33	0.40
RMP	0.48	0.35	0.54
PMN	0.43	1.01	0.44
PMP	0.44	0.44	0.43
TQP	0.96	0.90	0.51
TQS	0.96	0.89	0.44

Ideally, calibration loads would be parallel to principle axes of the balance coordinate system. In such a situation, for example, application of a calibration normal force would not apply any off-axis (side or axial) forces. Figure 24 shows the estimated axial and side forces due to applied normal force for all of the load combinations applied in configuration 2 based on photogrammetry measurements. The blue circles show the off-axis force due solely to the misalignment of the normal force linkage attachment points, which were measured immediately before and after the calibration test. The off-axis forces are proportional to the applied normal force, which in this configuration ranged from zero to 30,000 lb.

These off-axis forces might have been reduced if more time was expended in aligning the attachment points. However, the off-axis forces due to both alignment error and hardware deflection, shown as green crosses in Fig. 24, are much greater, which indicates that hardware deflection under load has much more influence. These points do not fall along a straight line, as the deflection offsets vary depending on which of the other calibration loads are being applied simultaneously with the normal force load.

Since one of the calibration goals was to keep applied force uncertainties to less than 5 lb, deflection measurements were a crucial part of the calibration process. Deflection data was acquired for all hardware configurations, but the deflection measurement results were similar between configuration 1 and 2. Therefore, the balance calibration data for configuration 2 will be used for the first wind tunnel entry. Figures 24-34 show the off-axis forces for all forces applied in configuration 2.

CONCLUDING REMARKS

This paper presented a new experimental capability to accurately measure changes to load vectors due to hardware deflections, which enables more accurate estimates of applied calibration loads. The challenges imposed by the TTR and calibration hardware were overcome by careful application of photogrammetry techniques. In addition, the misalignment measurements and selected deflection measurements results of the Tiltrotor Test Rig Balance 1.0 calibration were presented. The deflection measurement results are one part of the calibration process and do not reflect the final balance calibration. Accomplishments and findings are summarized below:

1. Digital photogrammetry was used to enhance NASA's capability to accurately calibrate large internal multi-component rotor balances.
2. The misalignments of the linkage attachment points were successfully measured before and after the calibration to estimate initial load application vectors.
3. The deflections of the linkage attachment points on the calibration body were successfully measured during the calibration to determine load vector changes due to applied loads.
4. Misalignment measurements and deflection measurements were both a crucial part of the TTR balance calibration process. Misalignment measurements alone would not have provided sufficient accuracy in estimating load vectors.
5. Off-axis forces (hardware interactions) were determined from deflection measurements for the three hardware configurations and for each load type.

ACKNOWLEDGMENTS

The authors wish to thank the TTR calibration crew of the National Full-Scale Aerodynamics Complex for enabling the calibration measurements. Particular thanks are extended to Alex Sheikman, Tom Norman, Alan Wadcock (NASA Ames) and Christopher Hartley (Jacobs Engineering). We also greatly appreciate the contributions of Gina Willink and James Kennon (NASA Ames) for their mechanical design work of the photogrammetry hardware. Last, but not least, Christine Gregg, Belen Veras-Alba, and Haley Cummings (NASA Ames Interns) for their contributions to the bench calibration of the photogrammetry system, Matthew Miller and Steve Gonzales for their support during the misalignment measurements (NASA Ames Interns) and Michelle Dominguez for her support during the deflection measurements (NASA Ames Intern).

REFERENCES

[1]van Aken, J. M., "Analysis of Calibration Data for the Multi-Component Rotor Balance Installed in the NFAC Large Rotor Test Apparatus," Paper AIAA 2007-146, 46th Aerospace Sciences Meeting and Exhibit, Reno, NV, January 8-11, 2007

[2]van Aken, J. M., Shinoda, P. M., Haddad, Farid, "Development of a Calibration Rig For Large Multi-Component Rotor Balance", 46th International Instrumentation Symposium of the Instrument Society of America, Bellevue, WA, April 30th – May 4th, 2010.

[3]Peterson, L. R., van Aken, J. M., "Dynamic Calibration of the NASA Ames Rotor Test Apparatus Steady/Dynamic Rotor Balance," NASA TM 110393, 1996

[4]Dold, J., Peipe, J., "High Resolution Data Acquisition to Observe Moving Objects," International Archives of Photogrammetry and Remote Sensing, Vol. XXXI, (Part 5B), Vienna, 1996

[5]Mikhail, E. M., Introduction to Modern Photogrammetry, John Wiley & Sons, Inc, New York, 2001.

[6]Wolf, P.R., Elements of Photogrammetry, McGraw-Hill, New York, 1974.

[7]Sandwith, Scott, and Cork, Glen, "V-STARS/M System Accuracy Test Results," Coordinate Measurement System Committee Conference, Dearborn, Michigan, July 31ST – Aug 4th, 2000.

Author contact:
Eduardo Solis eduardo.solis@nasa.gov
Larry Meyn larry.meyn@nasa.gov

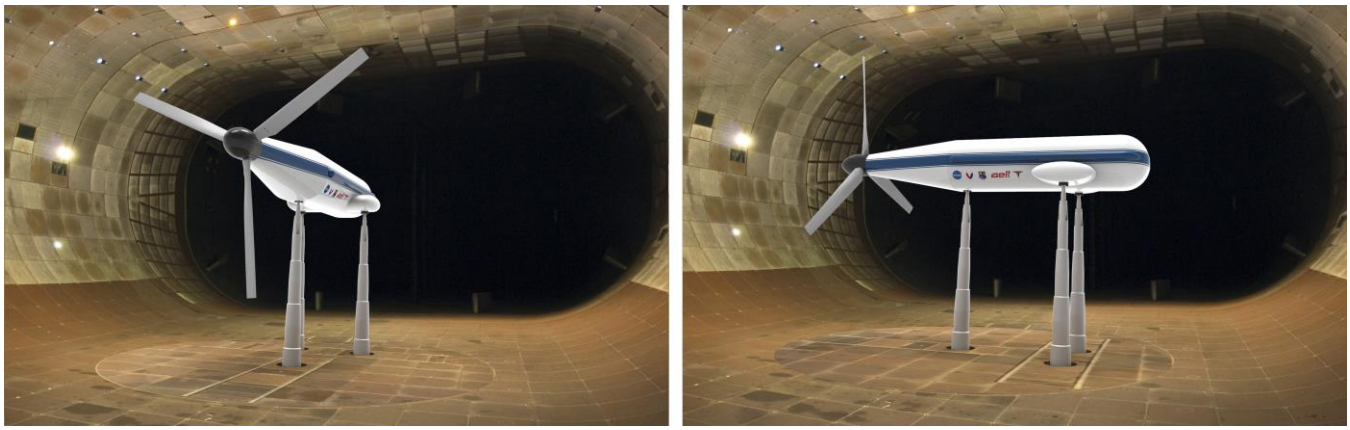

Figure 1. Renders of the TTR installed in the 40-by 80-Foot Wind Tunnel. (Left) Axial configuration. (Right) Edgewise configuration.

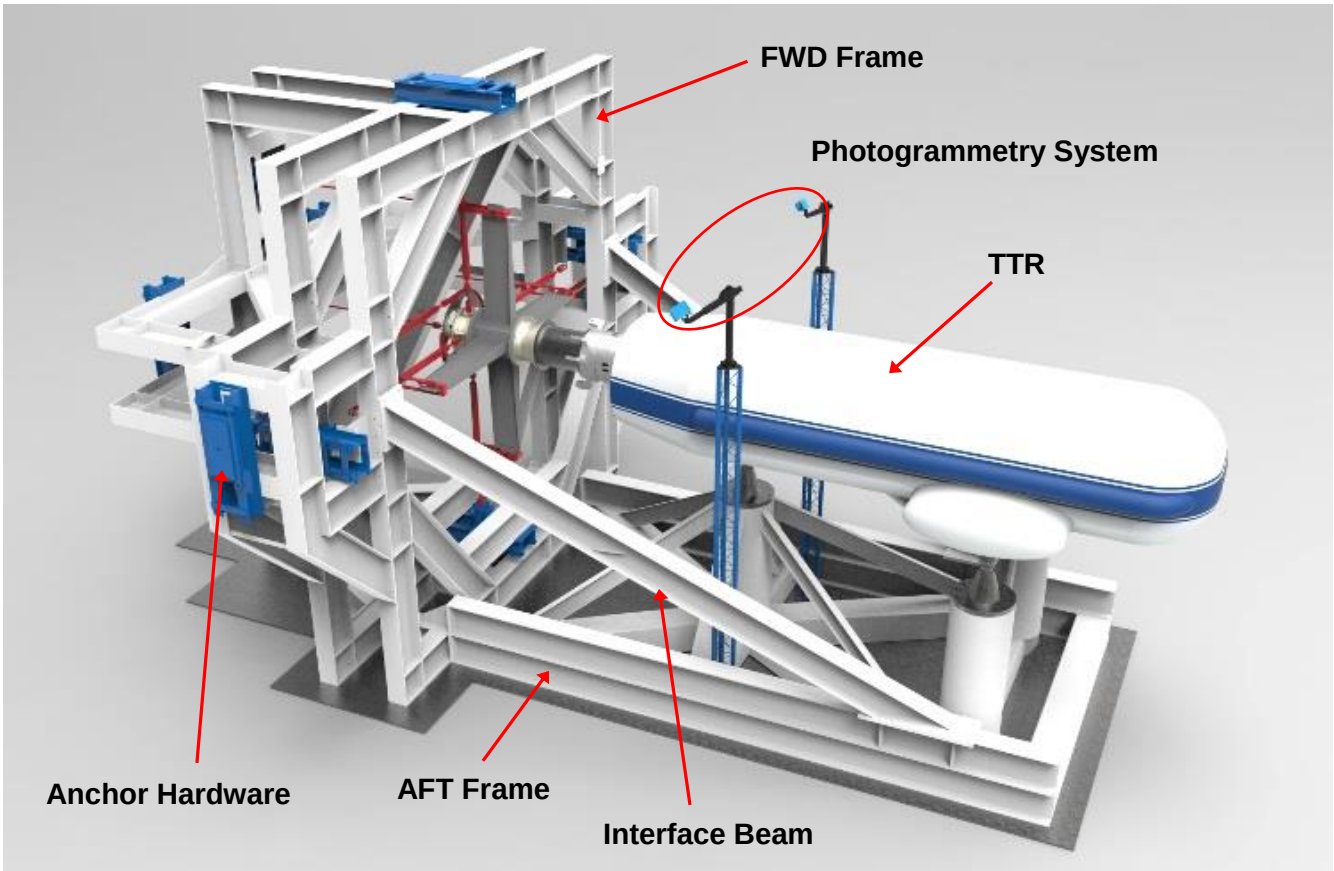

Figure 2. TTR installed on the calibration stand. The stairs and catwalks on the FWD Frame are removed to better reveal the design of the calibration stand.

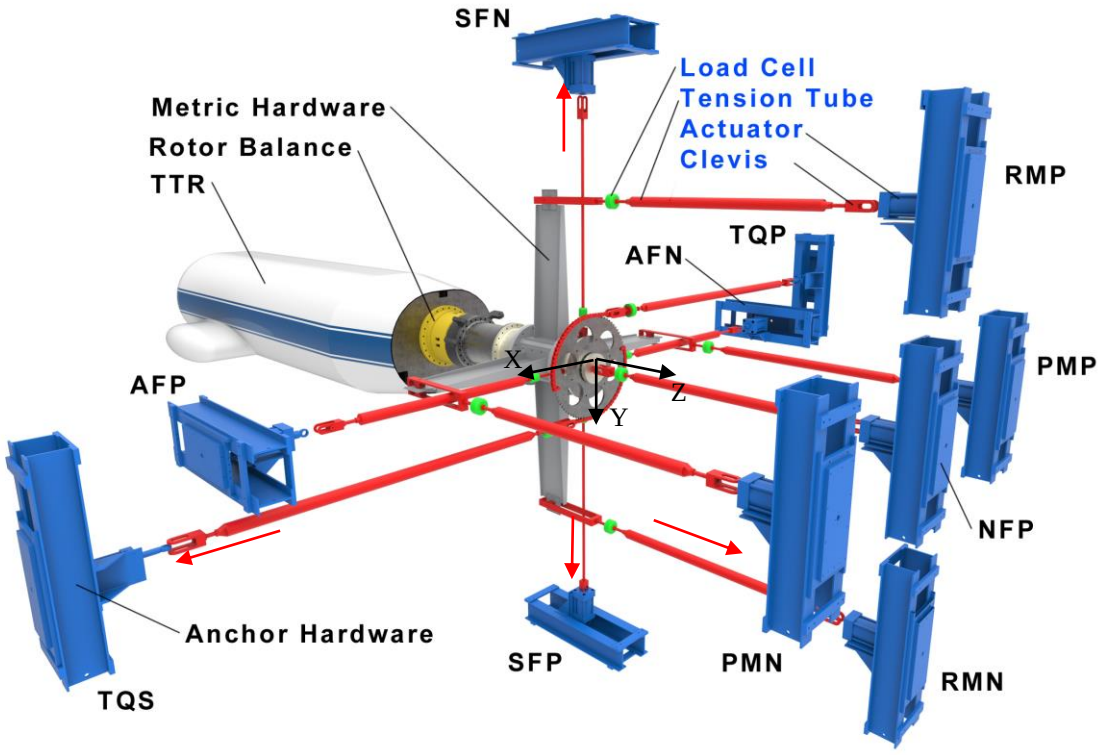

Figure 3. Calibration hardware loading tree with the FWD Frame and AFT Frame removed. Red arrows represent the load directions.

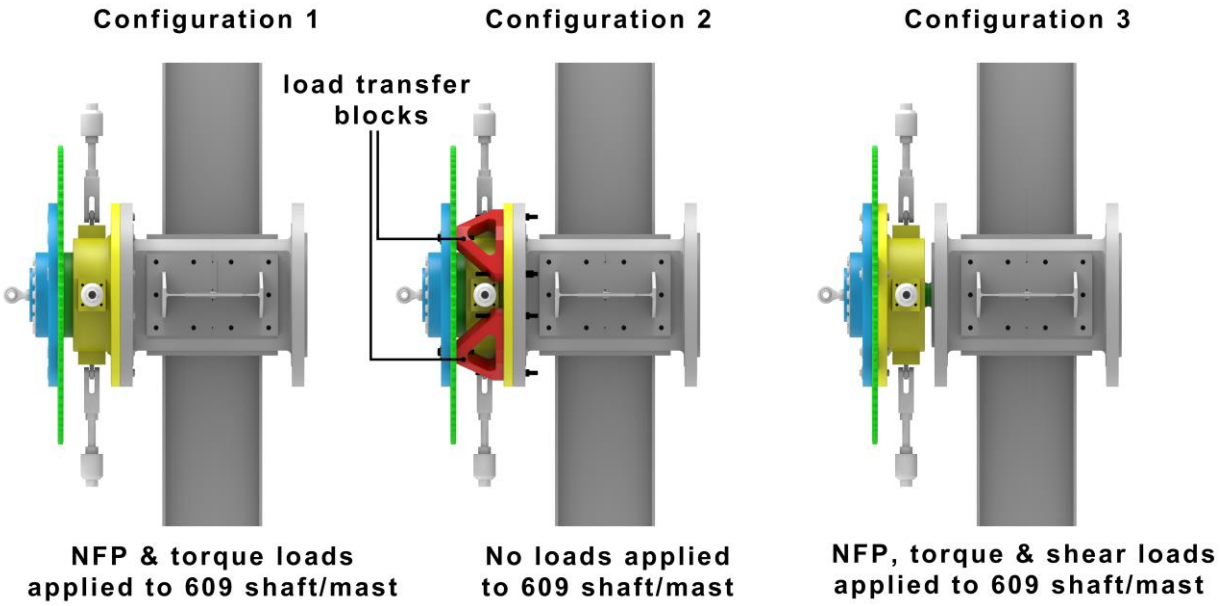

Figure 4. The forward hardware (in yellow), thrust adaptor plate (in blue), and the torque ring (in green) allowed for three loading configurations for the balance calibration process. Metric hardware is shown grey.

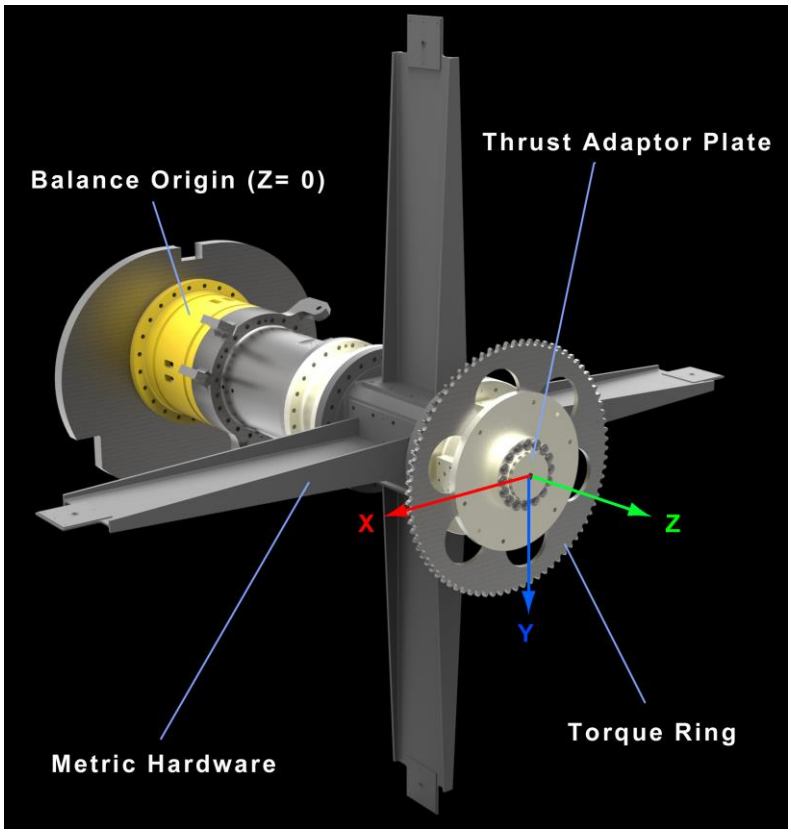

Figure 5. Balance calibration coordinate system. Balance origin z-axis = 0.

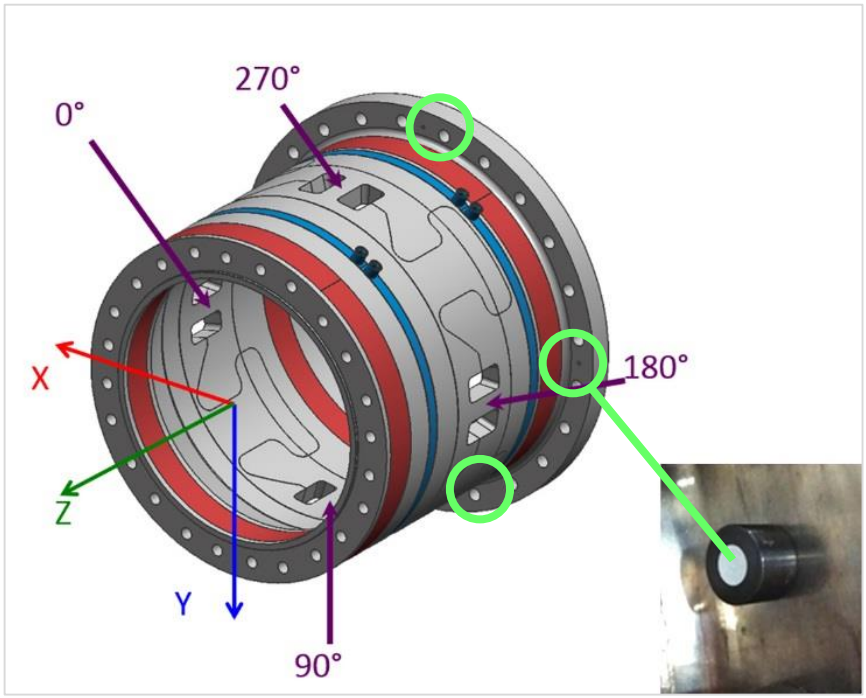

Figure 6. Green circles show the location for three of the four retro-reflective button targets installed on the flange of the rotor balance.

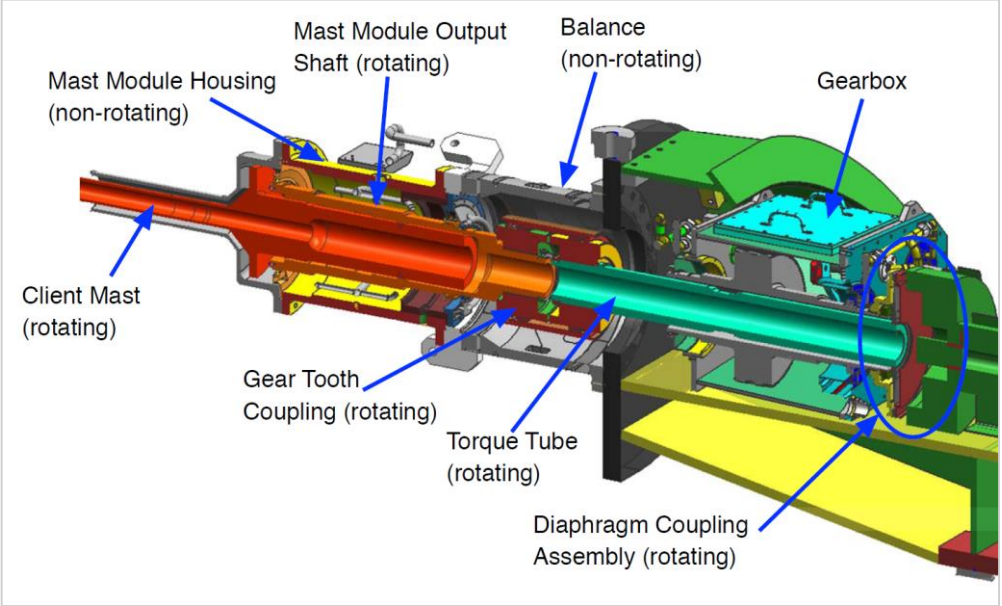

Figure 7. Torque tube and instrumented shaft flex-coupling are located in the fixed frame.

Figure 8. Bench calibration of the V-STARS/M system using a full-scale foam model of the metric hardware.

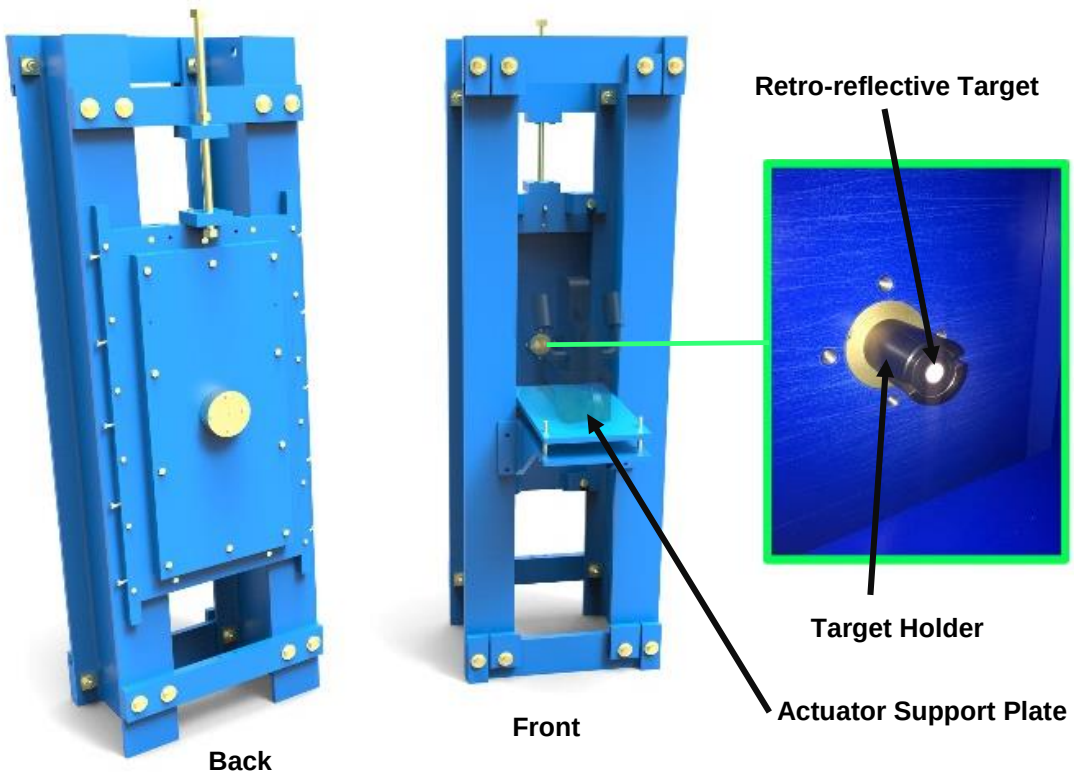

Figure 9. Anchor hardware design and target holder installation.

Figure 10. (Left) Roll moment linkage with custom button targets installed on each side of the moment arm. (Right) Shear block with retro-reflective button target.

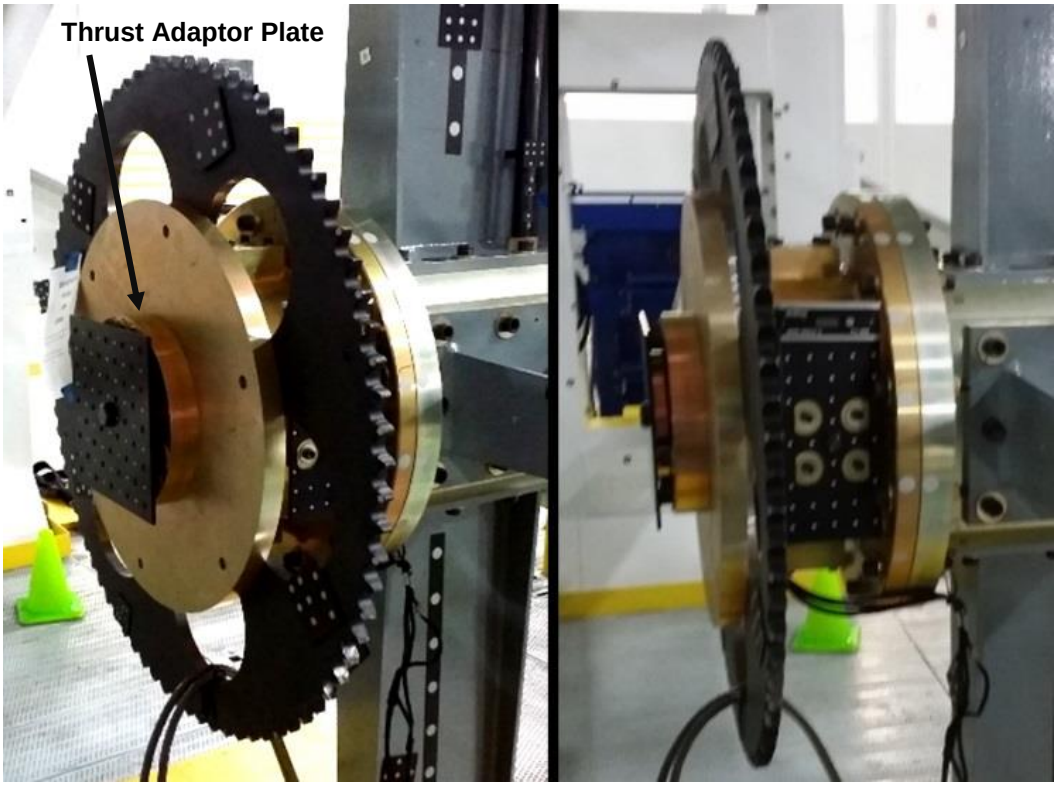

Figure 11. (Left) 12x12 inch plate installed on the thrust adaptor plate. (Right) 6x12 inch alignment plate installed on the axial negative shear block.

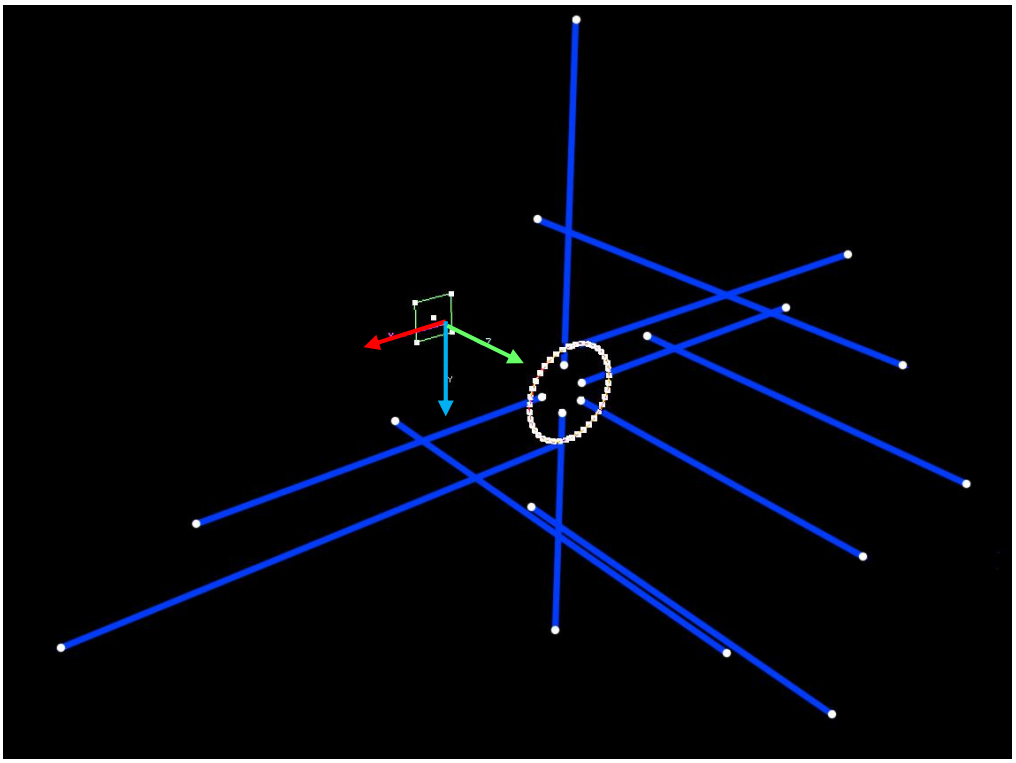

Figure 12. 3D measurement of the linkage attachment points. Blue lines represent the load vector between the linkage attachment points.

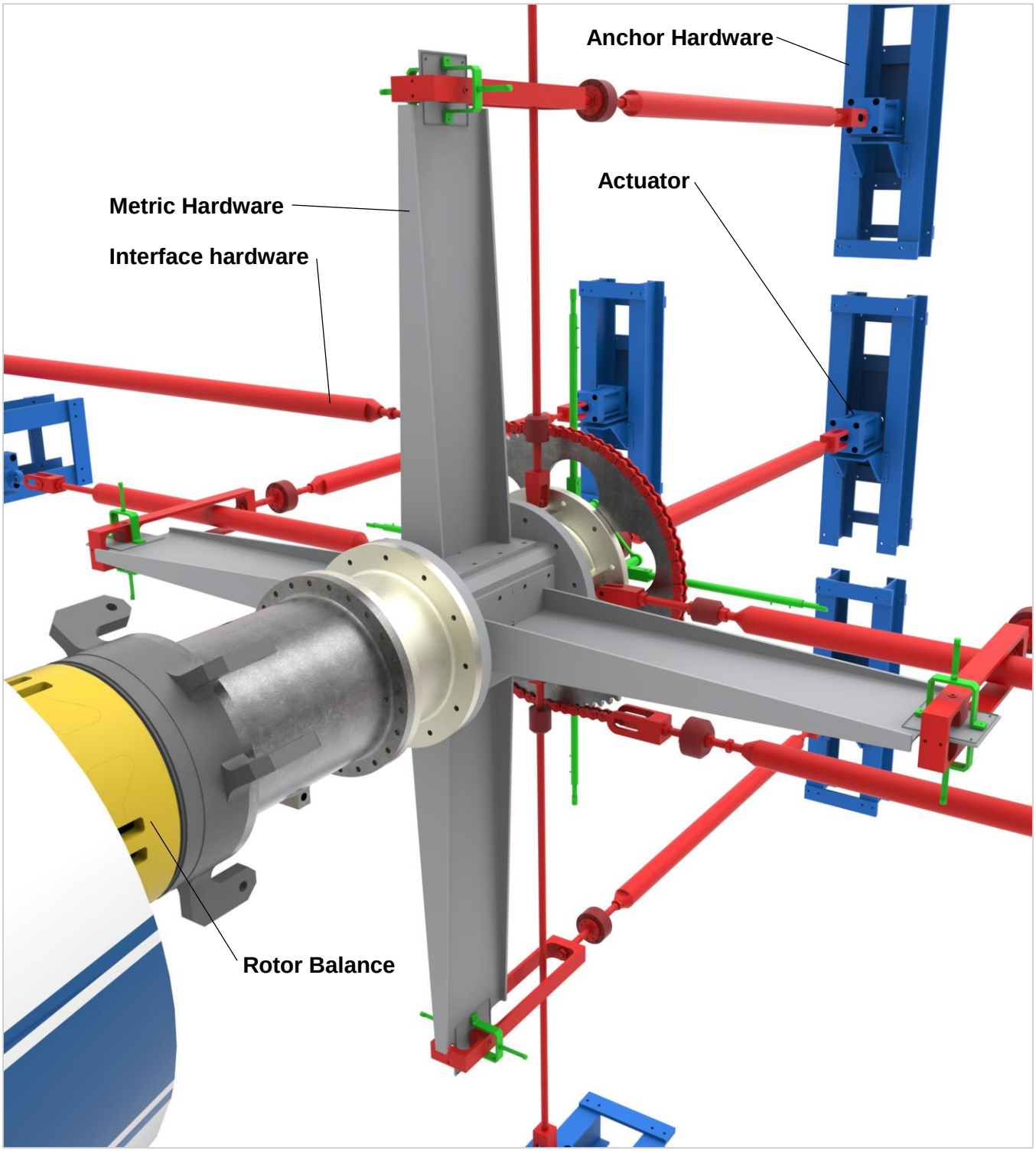

Figure 13. Interface hardware (red) attached to the moment arms on the metric hardware. Deflection hardware (green) installed around the interface hardware buildup.

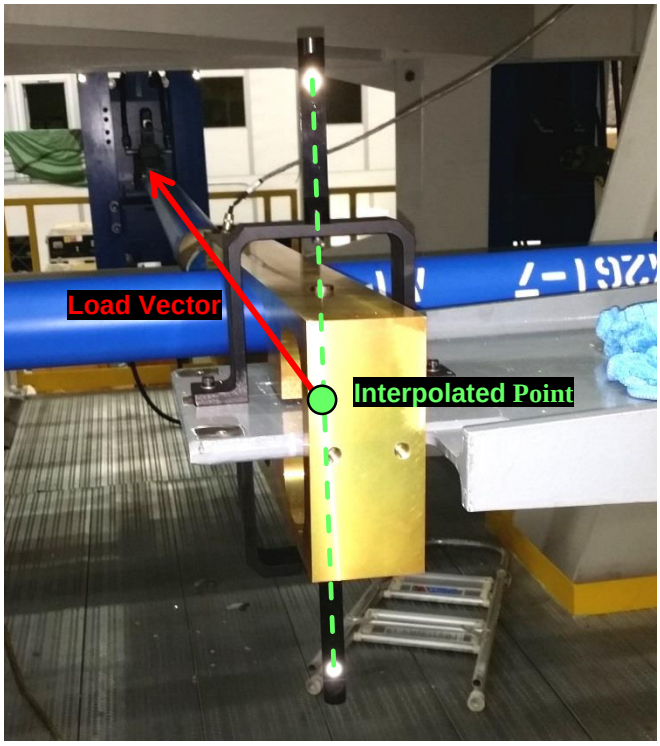

Figure 14. Extension bracket installed on each side of the moment arm.

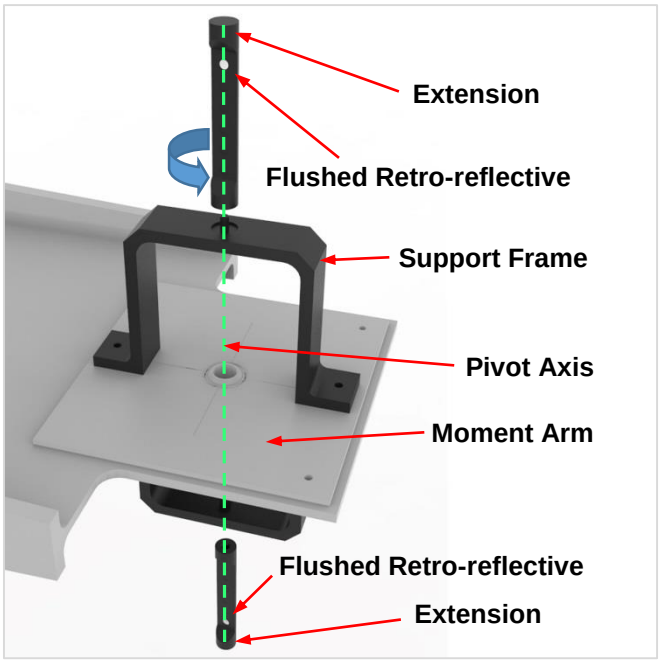

Figure 15. Exploded view of the extension bracket.

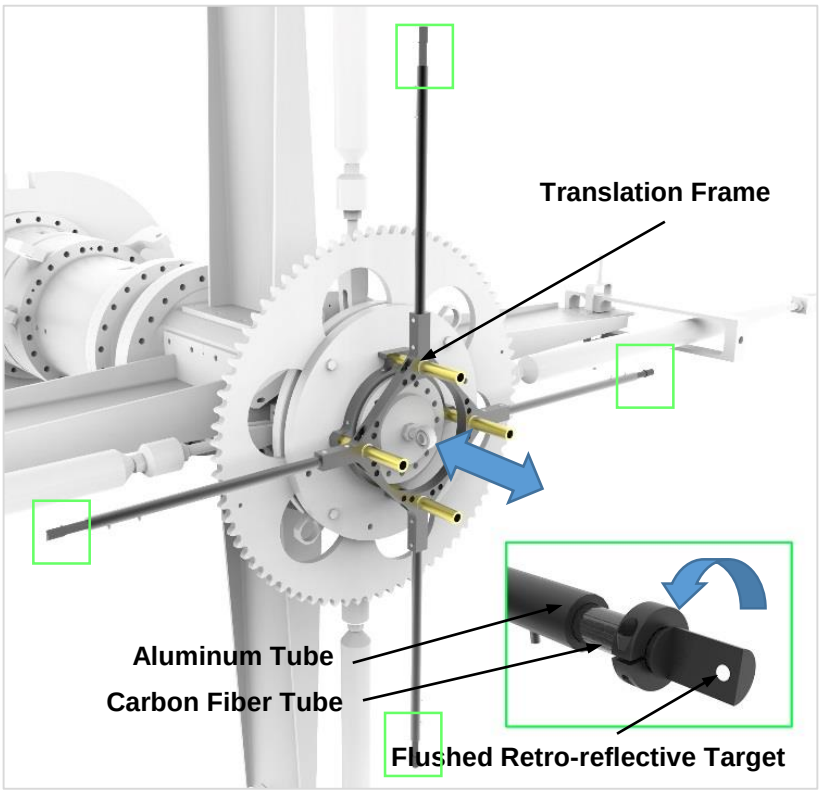

Figure 16. Deflection cross installed on the thrust adapter plate. Retro-reflective button targets installed on all four arms.

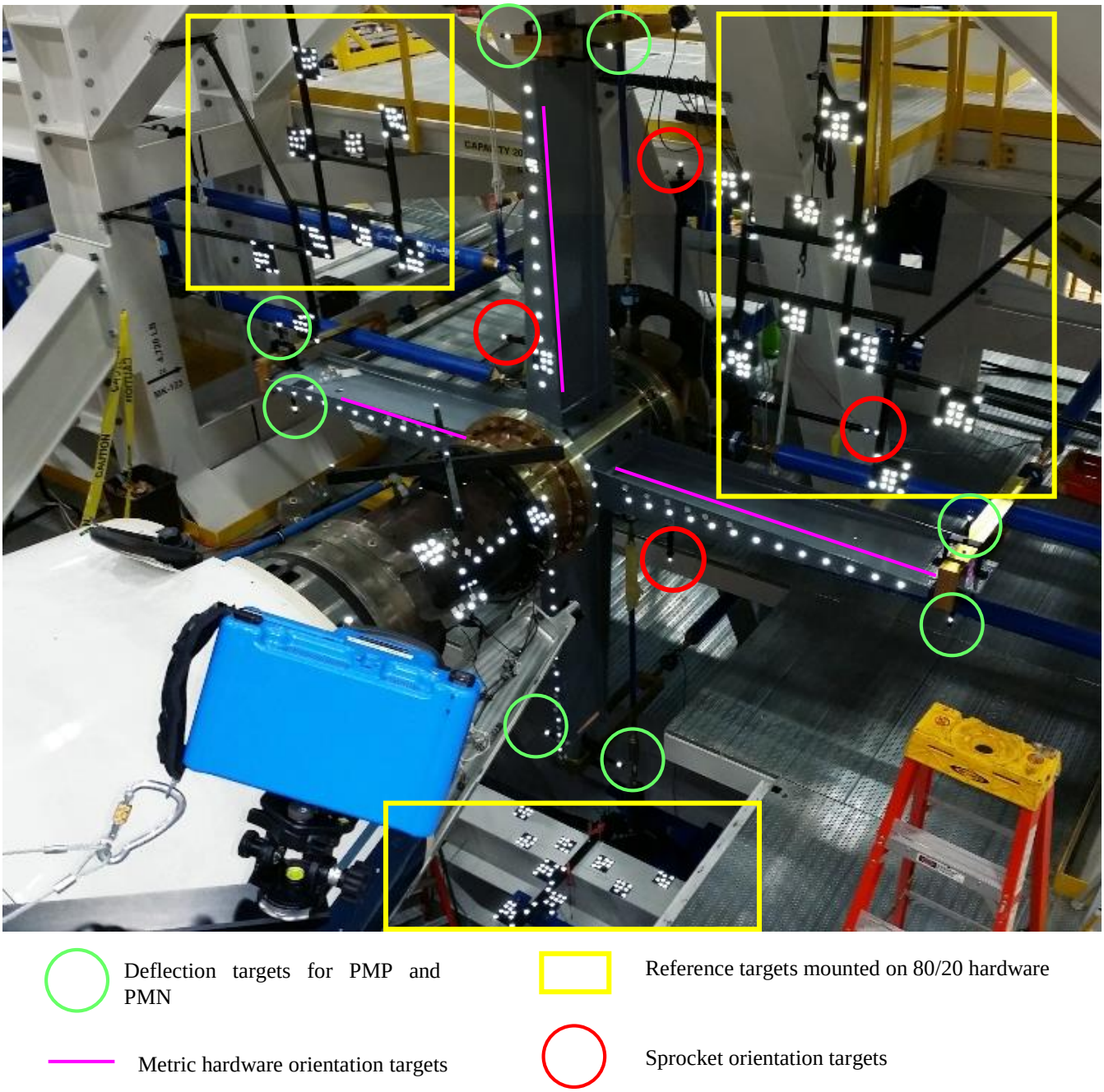

Figure 17. Deflection hardware installed on the FWD Frame and calibration body, which enabled retro-reflective target installation on the metric hardware.

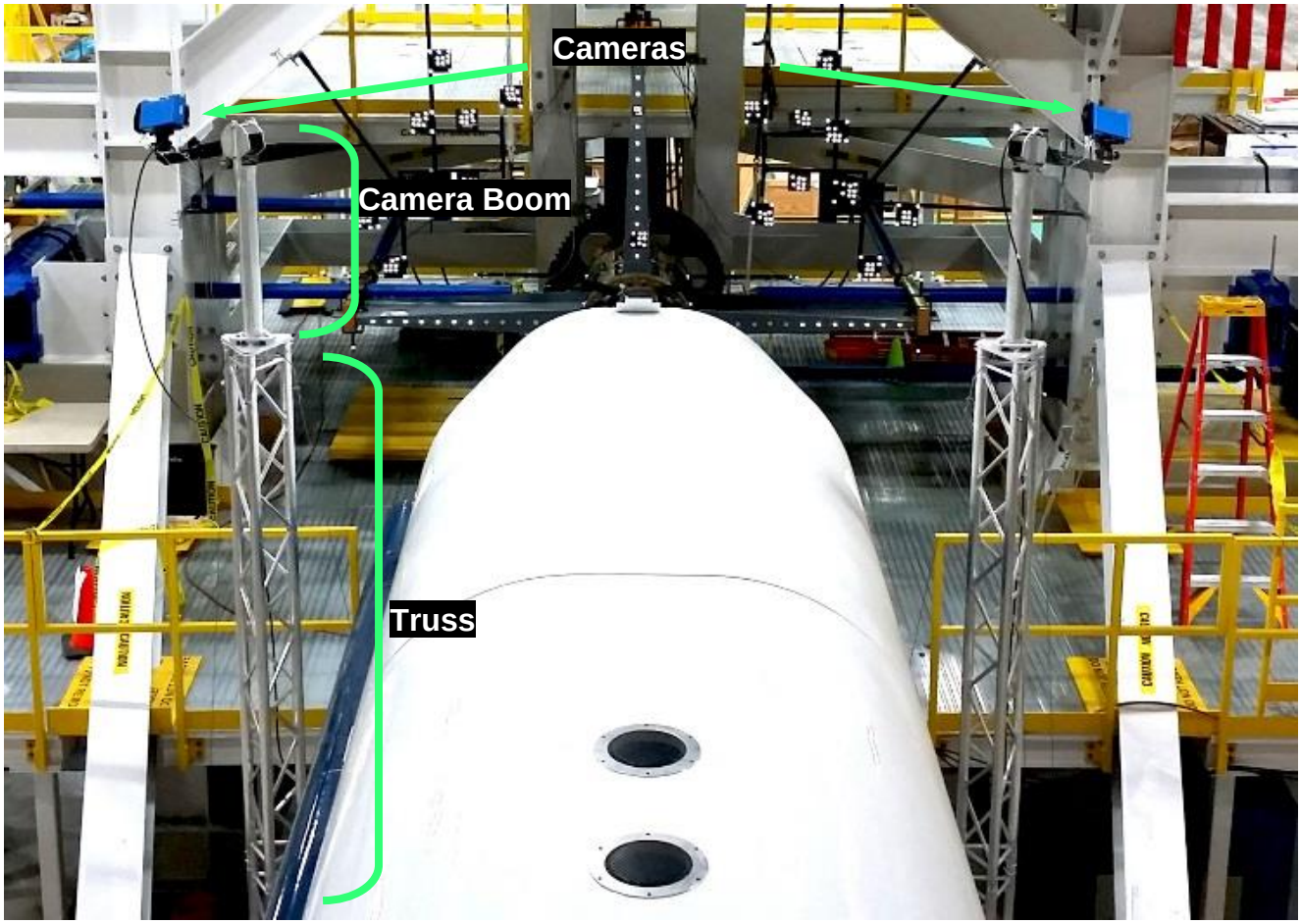

Figure 18. V-STARS/M system installed on the camera support structures.

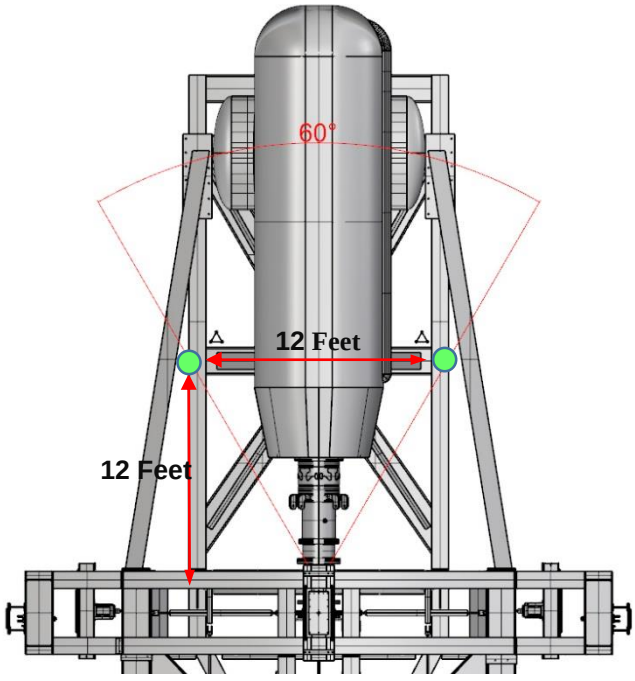

Figure 19. Plan view of the camera setup. Green dots represent the camera locations. 60 degree apex-angle.

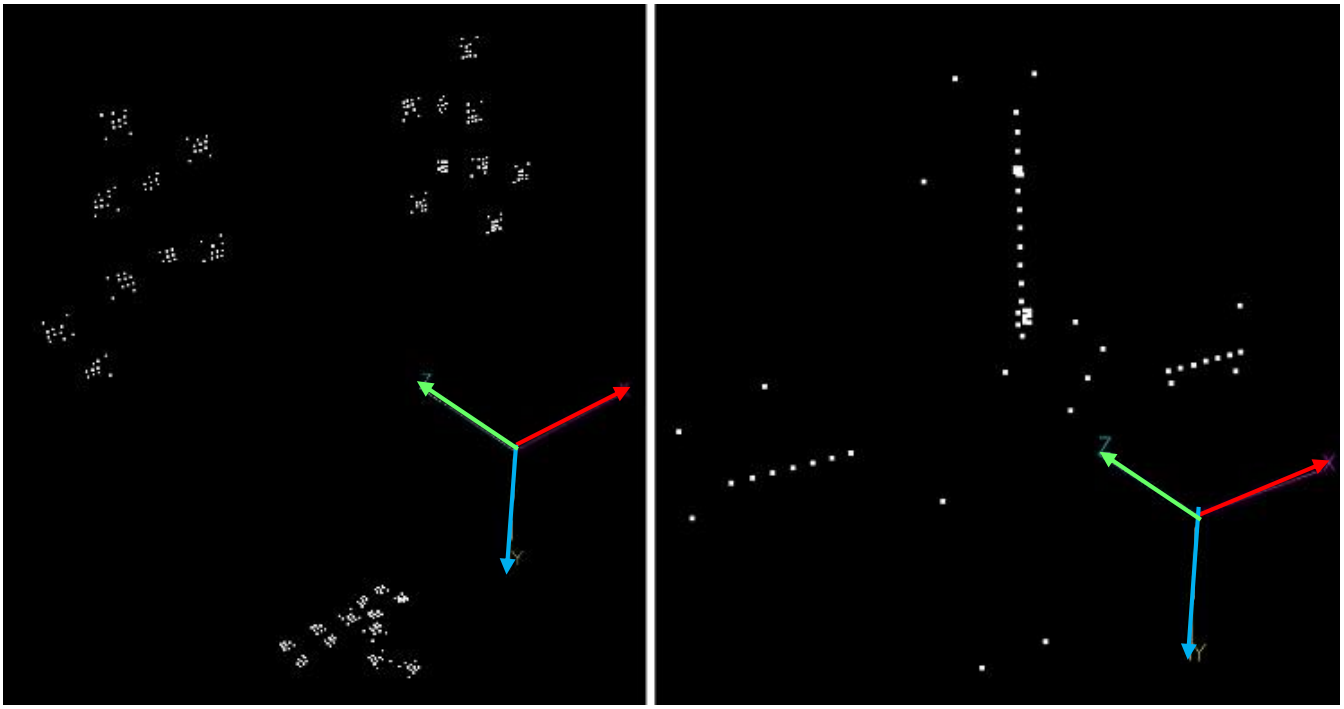

Figure 20. (Left) Driver (reference) points located on the FWD Frame. (Right) Detail (deflection) points located on the metric hardware.

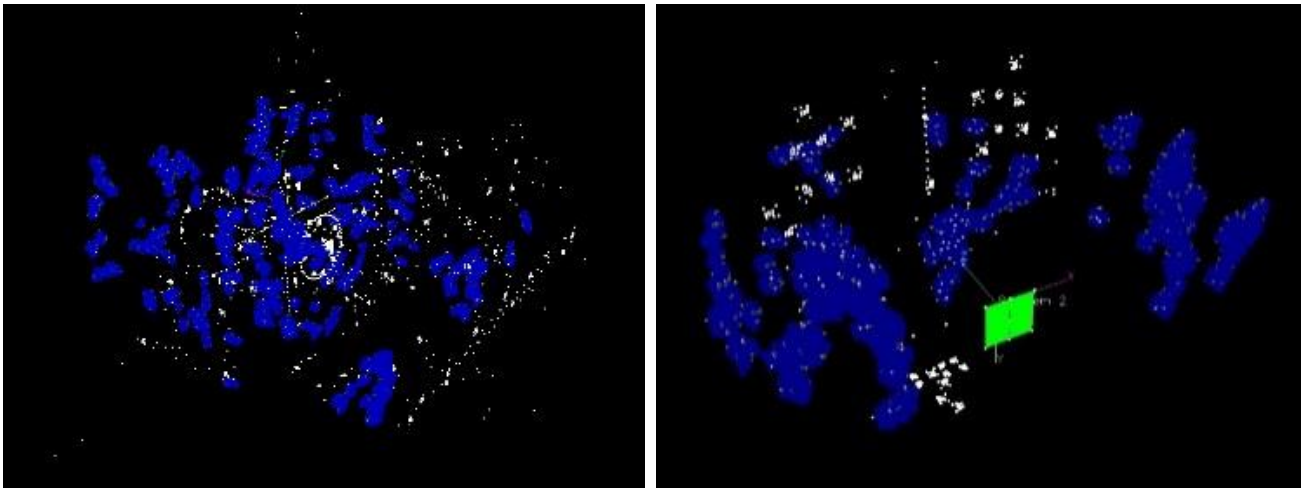

Figure 21. (Left) Camera stations used for the misalignment measurements. (Right) Camera stations used to generate the control field for the dual-camera system.

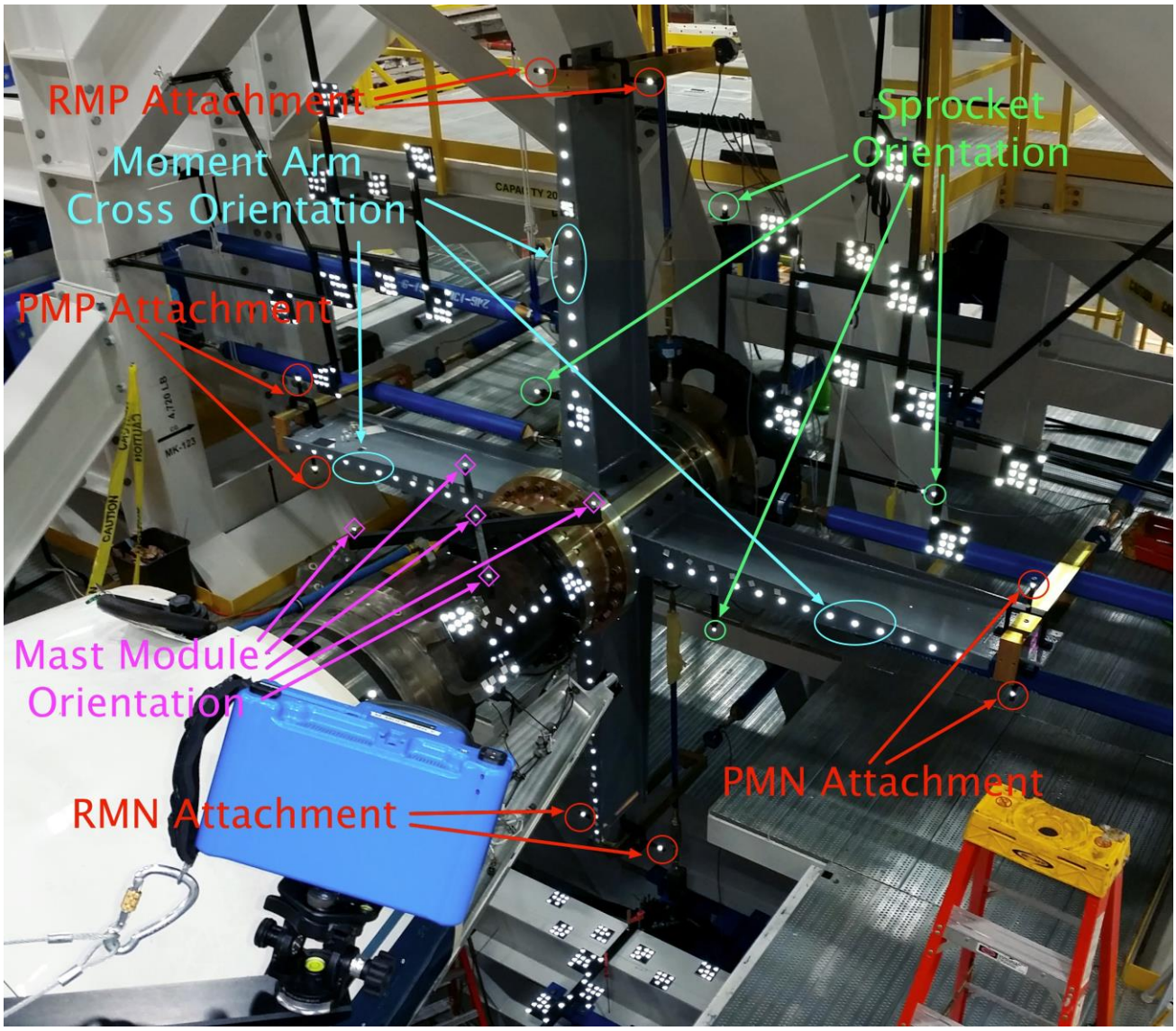

Figure 22. Retro-reflective targets used to interpolate the linkage attachment point locations.

Table 3. Pre-Balance Calibration Misalignment Measurement Results

	Forward Frame Attachment Points			Metric Hardware Attachment Points			Off-Axis Dimensions		
Actuator	X (in)	Y (in)	Z (in)	X (in)	Y (in)	Z (in)	X (in)	Y (in)	Z (in)
AFN	-157.3602	-0.2808	87.8699	-11.1297	0.0284	87.7536		-0.3092	0.1163
AFP	156.7434	0.3734	87.8736	11.1438	0.0347	87.7534		0.3387	0.1202
NFP	0.1814	0.5182	241.3603	0.0179	0.1143	99.7330	0.1635	0.4039	
PMN	70.7773	0.5607	241.5008	70.5028	0.0766	68.4881	0.2745	0.4841	
PMP	-70.2715	0.5009	241.4342	-70.4971	-0.0127	68.5067	0.2256	0.5136	
RMN	0.0316	71.0290	241.2030	-0.0311	70.5266	68.4788	0.0627	0.5024	
RMP	0.1237	-69.9057	241.4170	0.0375	-70.4707	68.5265	0.0862	0.5650	
SFN	0.1706	-149.6414	87.7872	0.0094	-11.1077	87.7584	0.1612		0.0288
SFP	-0.1263	131.9423	87.7221	0.0043	11.1625	87.7493	-0.1306		-0.0272
TQP	-202.1194	-22.5932	92.9346	0.0055	-22.2072	92.6242		-0.3860	0.3104
TQS	201.6462	22.8529	92.3419	0.0055	22.3728	92.6242		0.4801	-0.2823

Table 4. Post-Balance Calibration Misalignment Measurement Results

	Forward Frame Attachment Points			Metric Hardware Attachment Points			Off-Axis Dimensions		
Actuator	X (in)	Y (in)	Z (in)	X (in)	Y (in)	Z (in)	X (in)	Y (in)	Z (in)
AFN	-157.3932	-0.3134	87.8035	-11.1321	0.0020	87.7661		-0.3154	0.0374
AFP	156.6597	0.3610	87.8694	11.1515	0.0021	87.7694		0.3589	0.1000
NFP	0.1236	0.4442	241.4319	-0.0061	0.0738	100.0074	0.1297	0.3704	
PMN	70.6829	0.4816	241.4601	70.5040	0.0577	68.5103	0.1789	0.4239	
PMP	-70.3918	0.4253	241.3307	-70.5024	-0.0385	68.5194	0.1106	0.4638	
RMN	-0.0630	70.9286	241.4075	-0.0478	70.5110	68.5089	-0.0152	0.4176	
RMP	0.0367	-69.9889	241.4828	0.0433	-70.4962	68.5234	-0.0066	0.5073	
SFN	0.1171	-149.6585	87.7107	0.0015	-11.1304	87.7648	0.1156		-0.0541
SFP	-0.1862	131.8827	87.7322	0.0010	11.1441	87.7609	-0.1872		-0.0287
TQP	-202.2721	-22.6168	92.8580	-0.0007	-22.2379	92.6589		-0.3789	0.1991
TQS	201.7128	22.8316	92.3571	-0.0007	22.3371	92.6589		0.4945	-0.3018

Table 5. Average of the Pre-Balance and Post-Balance Calibration Misalignment Measurement Results

	Forward Frame Attachment Points			Metric Hardware Attachment Points			Off-Axis Dimensions		
Actuator	X (in)	Y (in)	Z (in)	X (in)	Y (in)	Z (in)	X (in)	Y (in)	Z (in)
AFN	-157.3767	-0.2971	87.8367	-11.1309	0.0152	87.7599		-0.3123	0.0769
AFP	156.7016	0.3672	87.8715	11.1477	0.0184	87.7614		0.3488	0.1101
NFP	0.1525	0.4812	241.3961	0.0059	0.0941	99.8702	0.1466	0.3872	
PMN	70.7301	0.5212	241.4805	70.5034	0.0672	68.4992	0.2267	0.4540	
PMP	-70.3317	0.4631	241.3825	-70.4998	-0.0256	68.5131	0.1681	0.4887	
RMN	-0.0157	70.9788	241.3053	-0.0395	70.5188	68.4939	0.0238	0.4600	
RMP	0.0802	-69.9473	241.4499	0.0404	-70.4835	68.5250	0.0398	0.5362	
SFN	0.1439	-149.6500	87.7490	0.0055	-11.1191	87.7616	0.1384		-0.0126
SFP	-0.1563	131.9125	87.7272	0.0027	11.1533	87.7551	-0.1589		-0.0280
TQP	-202.1958	-22.6050	92.8963	0.0024	-22.2226	92.6416		-0.3825	0.2548
TQS	201.6795	22.8423	92.3495	0.0024	22.3550	92.6416		0.4873	-0.2920

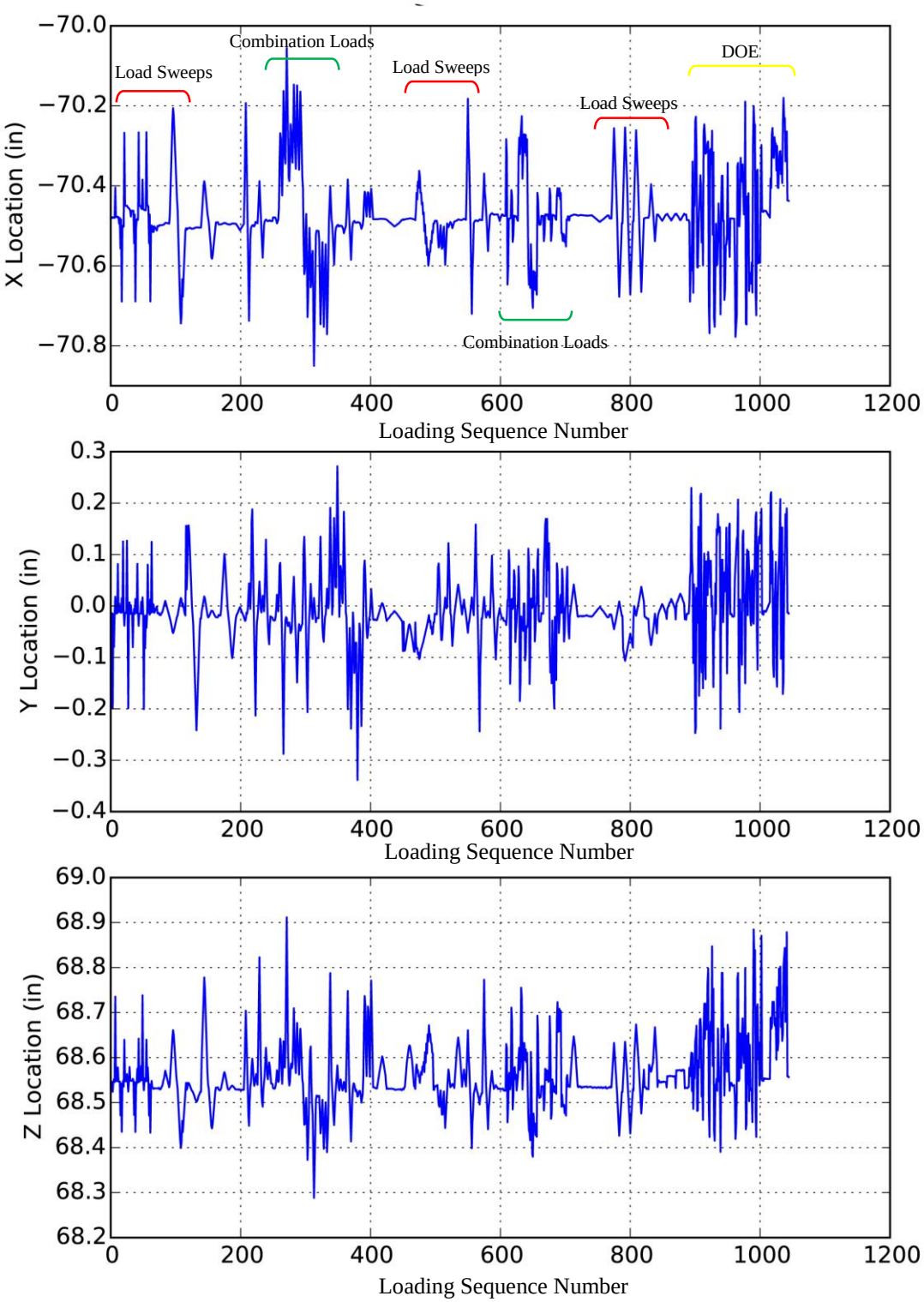

Figure 23. Deflection history for pitch moment positive interpolated point for all combination loads applied in configuration 1. Up to half an inch in lateral movement. Load application is in the Z-axis.

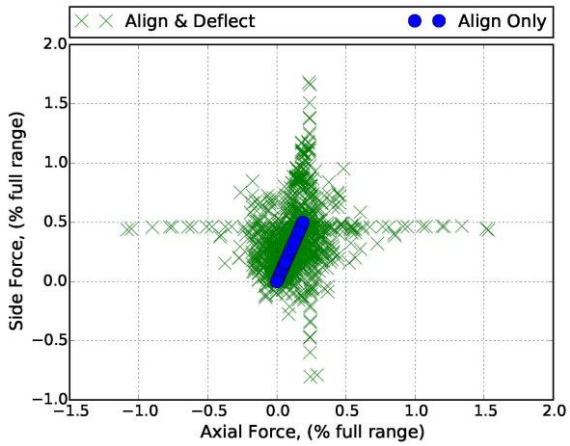

Figure 24. Side and axial forces due to misalignment of applied normal force for all load combinations in configuration 2.

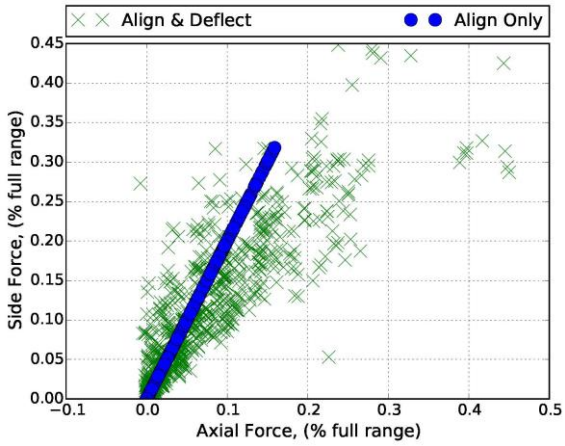

Figure 27. Side and axial forces due to misalignment of applied pitch moment negative force for all load combinations in configuration 2.

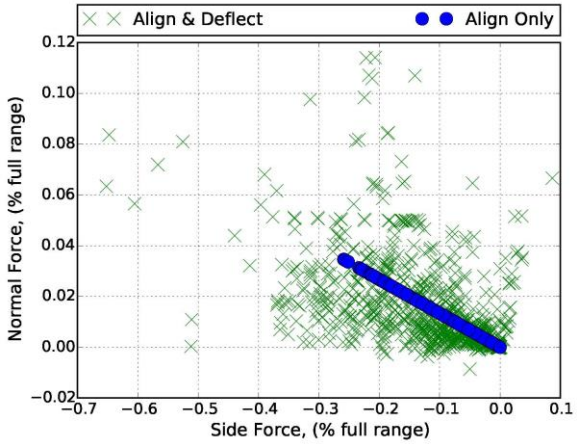

Figure 25. Normal and side forces due to misalignment of applied axial force negative for all load combinations in configuration 2.

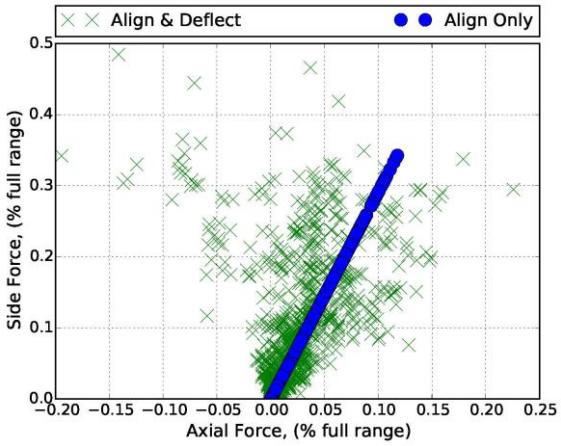

Figure 28. Side and axial forces due to misalignment of applied pitch moment positive force for all load combinations in configuration 2.

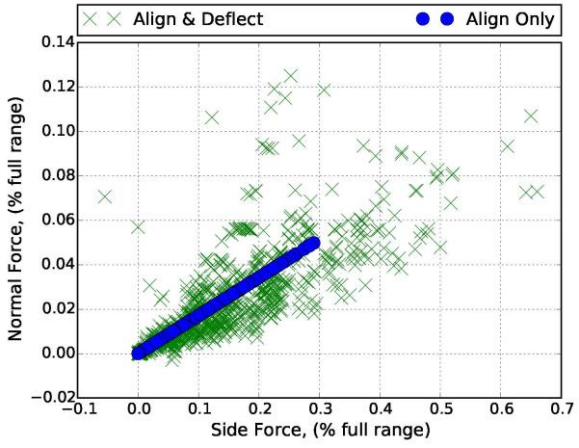

Figure 26. Normal and side forces due to misalignment of applied axial force positive for all load combinations in configuration 2.

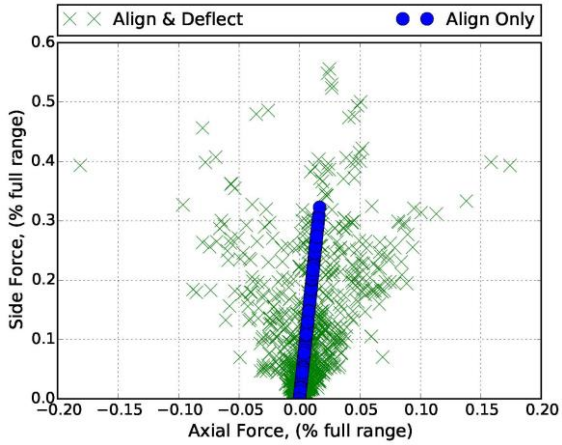

Figure 29. Side and axial forces due to misalignment of applied roll moment negative force for all load combinations in configuration 2.

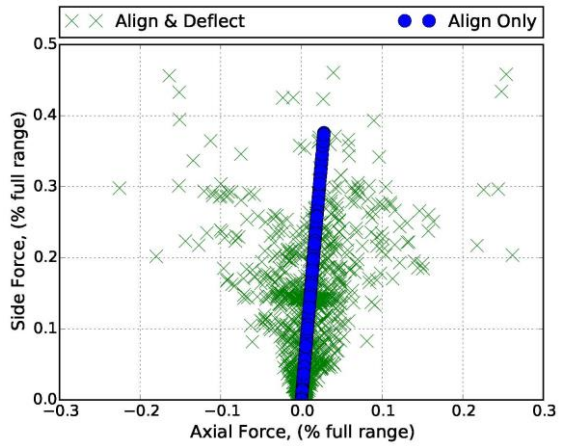

Figure 30. Side and axial forces due to misalignment of applied roll moment positive force for all load combinations in configuration 2.

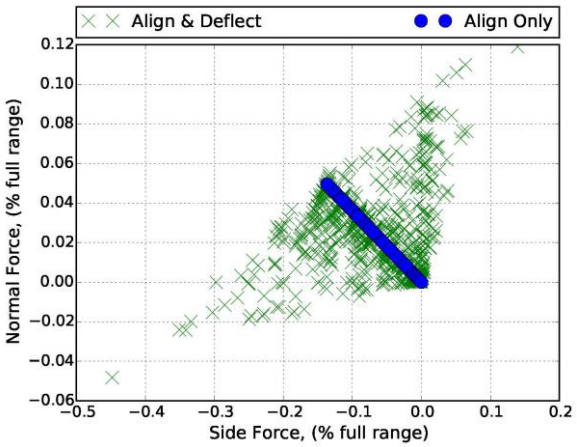

Figure 33. Normal and side forces due to misalignment of applied torque left force for all load combinations in configuration 2.

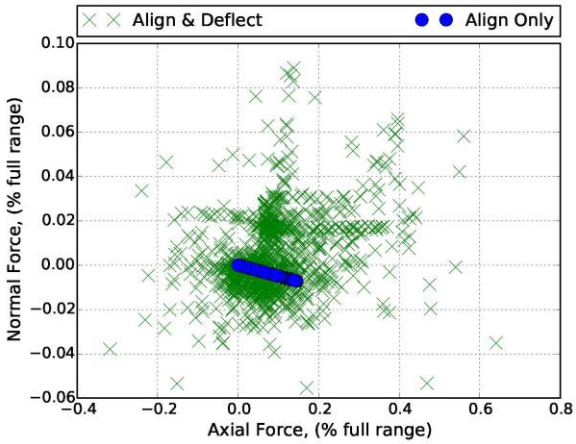

Figure 31. Normal and axial forces due to misalignment of applied side force negative for all load combinations in configuration 2.

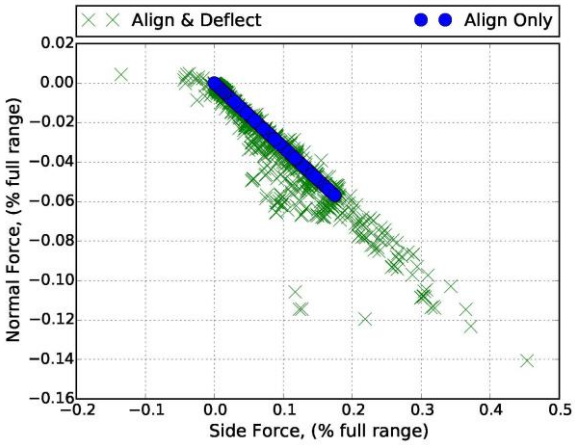

Figure 34. Normal and side forces due to misalignment of applied torque right force for all load combinations in configuration 2.

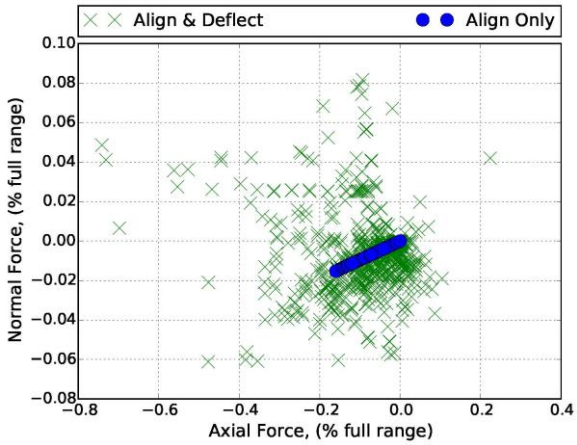

Figure 32. Normal and axial forces due to misalignment of applied side force positive for all load combinations in configuration 2.